JACS
JOURNAL OF THE AMERICAN CHEMICAL SOCIETY
Article
pubs.acs.org/JACS

Mechanistic Insight into Ketone α-Alkylation with Unactivated Olefins via C−H Activation Promoted by Metal−Organic Cooperative Catalysis (MOCC): Enriching the MOCC Chemistry

Yanfeng Dang,[†] Shuanglin Qu,[†] Yuan Tao,[†] Xi Deng,[†] and Zhi-Xiang Wang*[,†,‡]

[†]School of Chemistry and Chemical Engineering, University of the Chinese Academy of Sciences, Beijing 100049, China
[‡]Collaborative Innovation Center of Chemical Science and Engineering, Tianjin 300072, China

Supporting Information

ABSTRACT: Metal−organic cooperative catalysis (MOCC) has been successfully applied for hydroacylation of olefins with aldehydes via directed C(sp^2)−H functionalization. Most recently, it was reported that an elaborated MOCC system, containing Rh(I) catalyst and 7-azaindoline (**L1**) cocatalyst, could even catalyze ketone α-alkylation with unactivated olefins via C(sp^3)−H activation. Herein we present a density functional theory study to understand the mechanism of the challenging ketone α-alkylation. The transformation uses IMesRh(I)Cl(**L1**)(CH_2═CH_2) as an active catalyst and proceeds via sequential seven steps, including ketone condensation with **L1**, giving enamine **1b**; **1b** coordination to Rh(I) active catalyst, generating Rh(I)−**1b** intermediate; C(sp^2)−H oxidative addition, leading to a Rh(III)−H hydride; olefin migratory insertion into Rh(III)−H bond; reductive elimination, generating Rh(I)−**1c**(alkylated **1b**) intermediate; decoordination of **1c**, liberating **1c** and regenerating Rh(I) active catalyst; and hydrolysis of **1c**, furnishing the final α-alkylation product **1d** and regenerating **L1**. Among the seven steps, reductive elimination is the rate-determining step. The C−H bond preactivation via agostic interaction is crucial for the bond activation. The mechanism rationalizes the experimental puzzles: why only **L1** among several candidates performed perfectly, whereas others failed, and why Wilkinson's catalyst commonly used in MOCC systems performed poorly. Based on the established mechanism and stimulated by other relevant experimental reactions, we attempted to enrich MOCC chemistry computationally, exemplifying how to develop new organic catalysts and proposing **L7** to be an alternative for **L1** and demonstrating the great potential of expanding the hitherto exclusive use of Rh(I)/Rh(III) manifold to Co(0)/Co(II) redox cycling in developing MOCC systems.

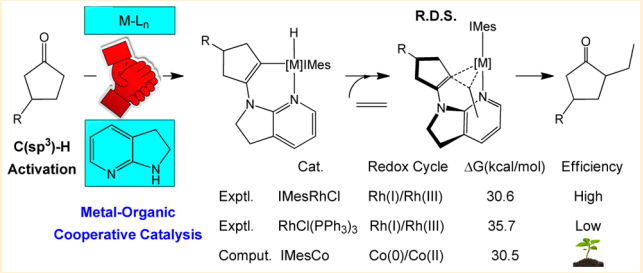

1. INTRODUCTION

The construction of C−C and C−heteroatom bonds via directed C−H bond functionalization is appreciated to be the "holy grail" in transition metal (TM) catalysis, attracting extensive research effort.[1−3] The addition of a C−H bond of ketone/aldehyde to olefins represents such a class of C−C bond forming reactions. A key issue for the addition is whether the carbonyl group can be an effective directing group (DG) to anchor a TM catalyst to cleave a targeted C−H bond. Exemplified by *ortho*-alkylation of aryl ketones and β-alkylation of α,β-unsaturated ketones developed by Murai and co-workers,[1e,4] carbonyl group could direct these sp^2 C−H bond functionalizations, but it is generally problematic in directing aldehyde sp^2 C−H bond activation due to decarbonylation.[5] To circumvent the problem, Jun et al. developed a conceptually new strategy,[6−9] known as metal−organic cooperative catalysis (MOCC),[8,10] which successfully promoted olefin hydroacylation with aldehyde. As illustrated in Scheme 1, the MOCC method wisely introduces an amine cocatalyst (e.g., 2-amino-3-picoline) to convert aldehyde to aldimine via acid-catalyzed condensation, thus installing a more effective N-containing DG to form a five-membered metallacycle.[6a,g,8] The in situ formed aldimine then undergoes imino C−H bond functionalization, leading to a ketimine which proceeds to the final hydroacylation product after acid-catalyzed hydrolysis. This strategy has been successfully applied to various reactions

Scheme 1. Illustration of Metal−Organic Cooperative Catalysis Strategy

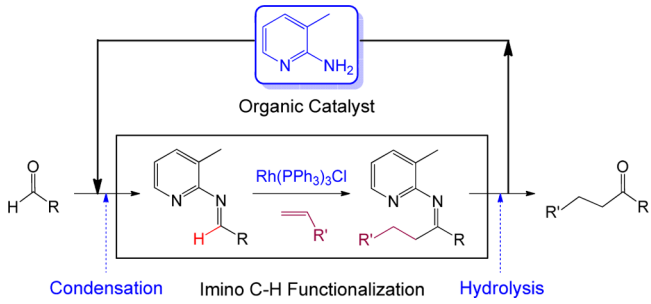

Received: February 13, 2015
Published: April 27, 2015

DOI: 10.1021/jacs.5b01502
J. Am. Chem. Soc. 2015, 137, 6279−6291

involving carbonyl group,[7,8] but direct coupling of simple ketones with unactivated olefins via sp^3 C−H activation remained to be a challenge[11] until Dong et al.'s 2012 report,[12] probably due to the inertness of the sp^3 C−H bond.

In 2012, Dong et al. advanced the MOCC strategy to achieve sp^3 C−H α-alkylation of 1,2-diketone with simple olefins (eq 1).[12] A wisdom of the strategy is that the condensation converts

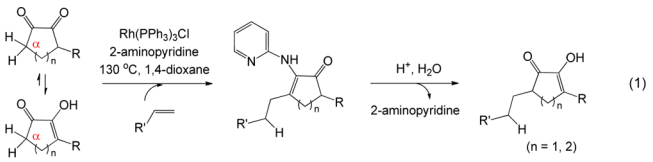

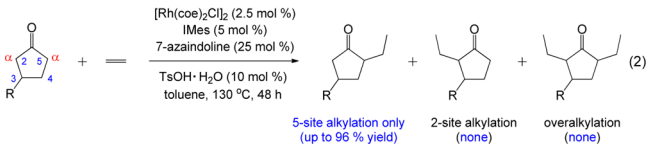

the inert sp^3 C^{α}−H bond to an enamine sp^2 C−H bond which is more reactive toward oxidative addition. Recently, they made another discovery.[13] By elaborating a MOCC system composing of $[Rh(coe)_2Cl]_2$ (coe = cyclooctene), 7-azaindoline (**L1**), *p*-toluenesulfonic acid (TsOH), and IMes NHC ligand (IMes =1,3-bis(2,4,6-trimethylphenyl)imidazol-2-ylidene), they accomplished α-alkylation of more general ketones with unactivated olefins via sp^3 C^{α}−H bond activation (e.g., eq 2).[13] Remarkably, the reaction only afforded monoalkylation product with complete regioselectivity and avoided overalkylation (eq 2).[13] The reaction represents a byproduct-free strategy to use cheap and readily available feedstocks under neutral conditions,[13] thus providing complementary compatibility to the conventional enolate alkylation chemistry. Looking into Dong et al.'s report and surveying previously developed MOCC systems, we were particularly intrigued by the following questions: (a) a MOCC system contains a TM catalyst and an organic cocatalyst. How does the duo collaborate and contribute to the transformation? (b) In their experimental study, Dong et al. also examined the Wilkinson's catalyst $RhCl(PPh_3)_3$ which was commonly used as the metal component of MOCC in aldehyde alkylation, but the catalyst performed poorly in catalyzing the ketone α-alkylation, thus raising a question why the new MOCC system worked so efficiently. (c) Dong et al. examined several amine cocatalysts, but only 7-azaindoline (**L1**) acted efficiently, whereas others delivered no product at all, thus raising a question why **L1** is so unique and how to identify an effective organic cocatalyst. And (d) all reported MOCC systems used the Rh(I)/Rh(III) redox manifold to complete a catalytic cycle. Can other transition metals with the same/or alternative redox cycling (e.g., Co(I)/Co(III) or Co(0)/Co(II) in particular) be utilized in MOCC? In this study, we relied on density functional theory (DFT) computations to gain insight into the mechanism (a), which allows us to solve the experimental puzzles (b) and (c). To enrich MOCC chemistry, on the basis of our mechanistic understanding and other relevant experimental evidence, we explored the possibility of (d). The mechanism with energetic and geometric details allows chemists to "visualize" the reaction, thus helping them to invent new MOCC systems. Our proposed new MOCC system could serve as stimulus or basis for experimental realizations.

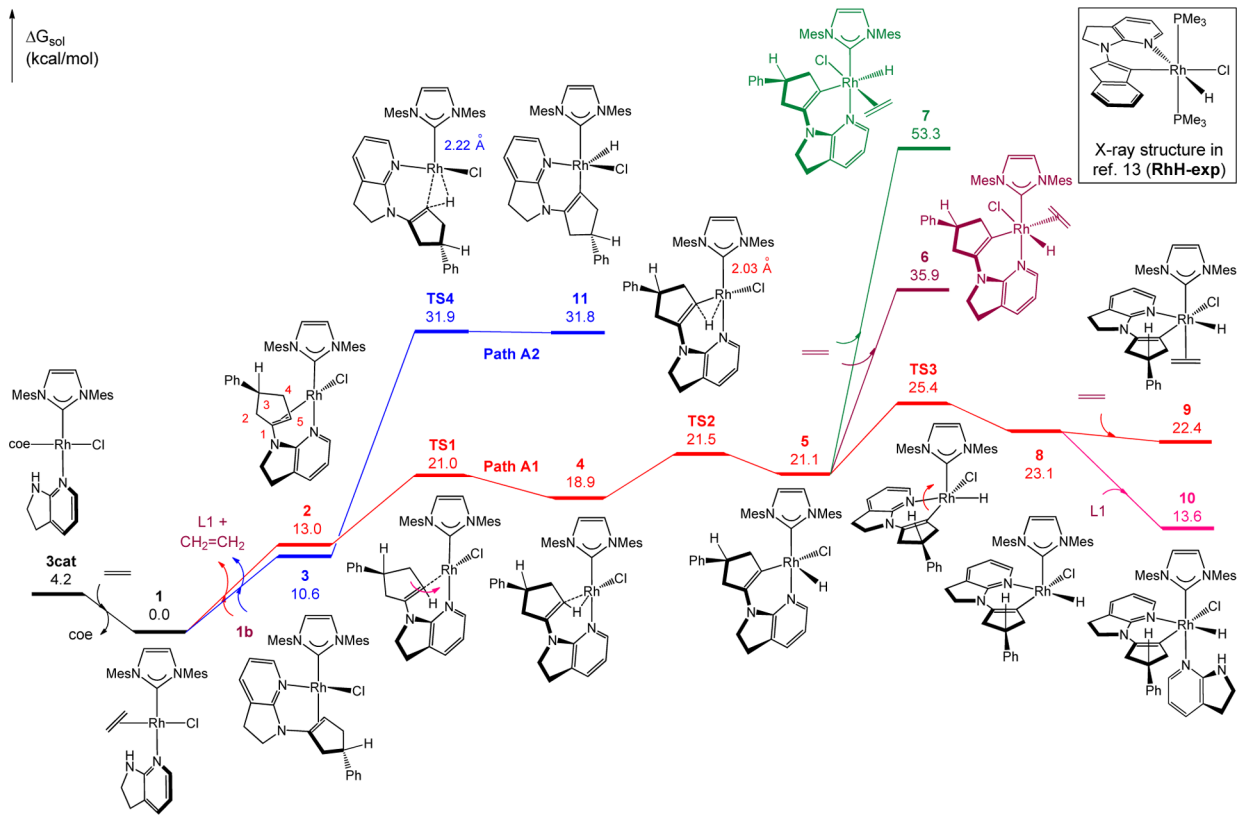

Figure 1. Free energy profiles for the alkylation of enamine **1b** with ethylene mediated by **3cat**. Energies are relative to **1** + **1b** and are mass balanced.

DOI: 10.1021/jacs.5b01502
J. Am. Chem. Soc. 2015, 137, 6279−6291

2. COMPUTATIONAL METHODS

Actual catalysts and substrates were employed in performing all the standard DFT computations. Geometries were optimized and characterized by frequency analysis calculations to be minima or transition states (TSs) at the B3LYP[14]/BSI level in the gas phase, where BSI denotes a basis set combining SDD[15] for rhodium and 6-31G(d,p) for nonmetal atoms. The energies were then improved by M06[16]/BSII//B3LYP//BSI single-point energy calculations with solvent effects simulated by the SMD[17] solvent model, using the experimental solvent (toluene). The combined use of M06 and B3LYP has been successfully applied to investigate various transition-metal-catalyzed reactions.[18,19] In the present study, we further validated that the B3LYP/BSI optimized geometry of a Rh(III)−H hydride (i.e., **RhH-exp** in Figure 1) is in good agreement with its X-ray structure[13] and those optimized at the M06/BSI and M06/BSII levels (see Figure S1). The refined energies were corrected to enthalpies and free energies at 298.15 K and 1 atm, using the gas phase B3LYP/BSI harmonic frequencies. Free energies (in kcal/mol) obtained from the M06/BSII//B3LYP/BSI calculations were discussed. All calculations were carried out with the Gaussian 09 program.[20] Additional computational results, energies, and Cartesian coordinates of the optimized structures are given in the Supporting Information.

3. RESULTS AND DISCUSSION

In this study, we chose the standard experimental α-alkylation of 3-phenylcyclopentanone **1a** with ethylene as a representative system (i.e., R = Ph in eq 2) to compute the mechanism, on which we understand the regioselectivity and chemoselectivity of the reaction (subsection 3.1). On the basis of the established mechanism, we investigate the effects of various factors on the α-alkylation, including the organic cocatalysts in subsection 3.2, ligand (PPh_3) in subsection 3.3, and Co(0)/Co(II) redox mainfold in subsection 3.4.

3.1. Mechanism and Origins for Regioselectivity and Reactivity. *Mechanism.* The complex $[Rh(coe)_2Cl]_2$ **1cat** is a precursor, requiring to be initiated to the active catalyst. Scheme 2 depicts our proposed mechanism for **1cat** initiation.

Scheme 2. Initiation of the Precatalyst 1cat $[Rh(coe)_2Cl]_2$

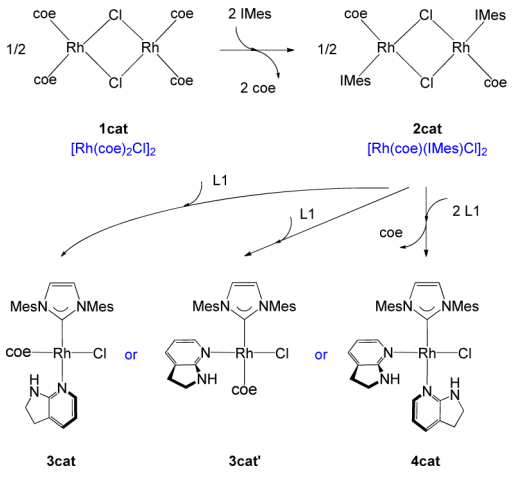

First, the bimetallic Rh(I) precursor undergoes ligand substitution for IMes ligands, generating the bimetallic **2cat** with an energy release of 37.0 kcal/mol. Supportively, **2cat** has been prepared by James' group[21a] and the substitution has also been demonstrated to proceed in different catalytic systems that used the same Rh(I) precursor and NHC ligand.[21a,b,d] Subsequently, **2cat** further undergoes substitution for 7-azaindoline (**L1**), which could lead to monometallic **3cat**, **3cat′**, or **4cat**. Although the generation of **3cat′** is endergonic by 0.9 kcal/mol, the generations of **3cat** and **4cat** are exergonic by 2.9 and 2.7 kcal/mol, respectively, indicating the feasibility of the initiation process. We used the most stable **3cat** as the initial active species to compute the catalytic mechanism. Notably, an analogue of **3cat** has been isolated crystallographically.[21d,e] It should be pointed out that using **3cat′** and **4cat** would not give a different mechanism, because both ligands in these species will be replaced (vide infra).

Racemic (*R*/*S*)-**1a** was used in the experimental study. Due to the symmetric feature of IMes ligand, the energy profiles using (*R*)- and (*S*)-**1a** should be identical. Thus, we only need to take one of the enantiomers (e.g., (*S*)-**1a**) into consideration. For simplicity, we hereafter will not specify the (*S*)-chirality. It is well-known that ketone and secondary amine can condense feasibly under the catalysis of Bronsted acids (e.g., TsOH used in the experiment) forming enamine. The condensation of ketone **1a** and secondary amine (**L1**) can result in two different enamines, namely, **1b** with $C^1{=}C^5$ double bond formed or **1b′** with $C^1{=}C^2$ double bond formed (Scheme 3). Computations

Scheme 3. Regioselectivity of α-Alkylation of 3-Phenylcyclopentanone 1a with Ethylene[a]

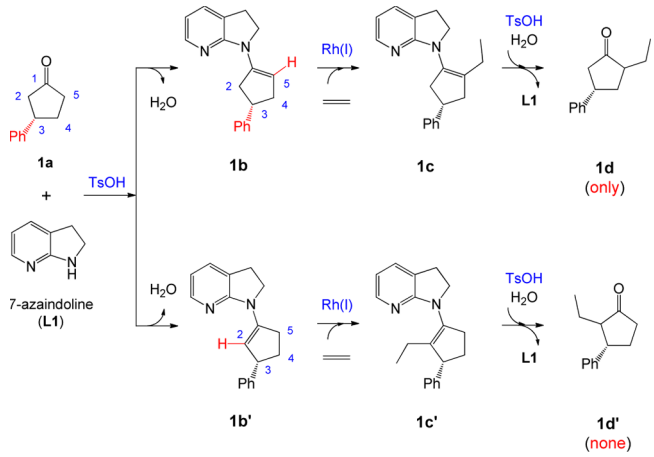

[a]Note that we only considered (*S*)-**1a** in the whole study (see text).

show that the TsOH-catalyzed condensation of **1a** with **L1** giving **1b** and **1b′** is kinetically favorable and endergonic by 7.3 and 6.9 kcal/mol, respectively (see Figure S2 for details). The less stable **1b** than **1b′** does not coincide with the experimental product of **1d** via 5-site α-alkylation rather than **1d′** via 2-site α-alkylation. Therefore, the regioselectivity must be kinetically controlled by the late stage involving TM catalyst (vide infra). Since the condensations are endergonic, as transient species, enamines **1b** and **1b′** are only available via microscopic equilibrium, indicating that high concentration of **L1** would greatly benefit the transformation. Consistently, Dong et al. observed that decreasing **L1** concentration from 50% to 25% lowered the yield of the product from >99% to 63% in 24 h (see Table S1 in ref 13). Because the experimental product **1d** correlates with **1b**, we discuss the mechanism using the **3cat**-catalyzed **1b** alkylation, and then elucidate why **1b′** cannot give corresponding product (**1d′**).

The pathway for enamine **1b** alkylation (i.e., **1b** → **1c** in Scheme 3) catalyzed by **3cat** is displayed in Figures 1 and 2, along with the relative free energies and key geometric parameters. Note that, because of the chirality of **1b**, there is

DOI: 10.1021/jacs.5b01502
J. Am. Chem. Soc. 2015, 137, 6279−6291

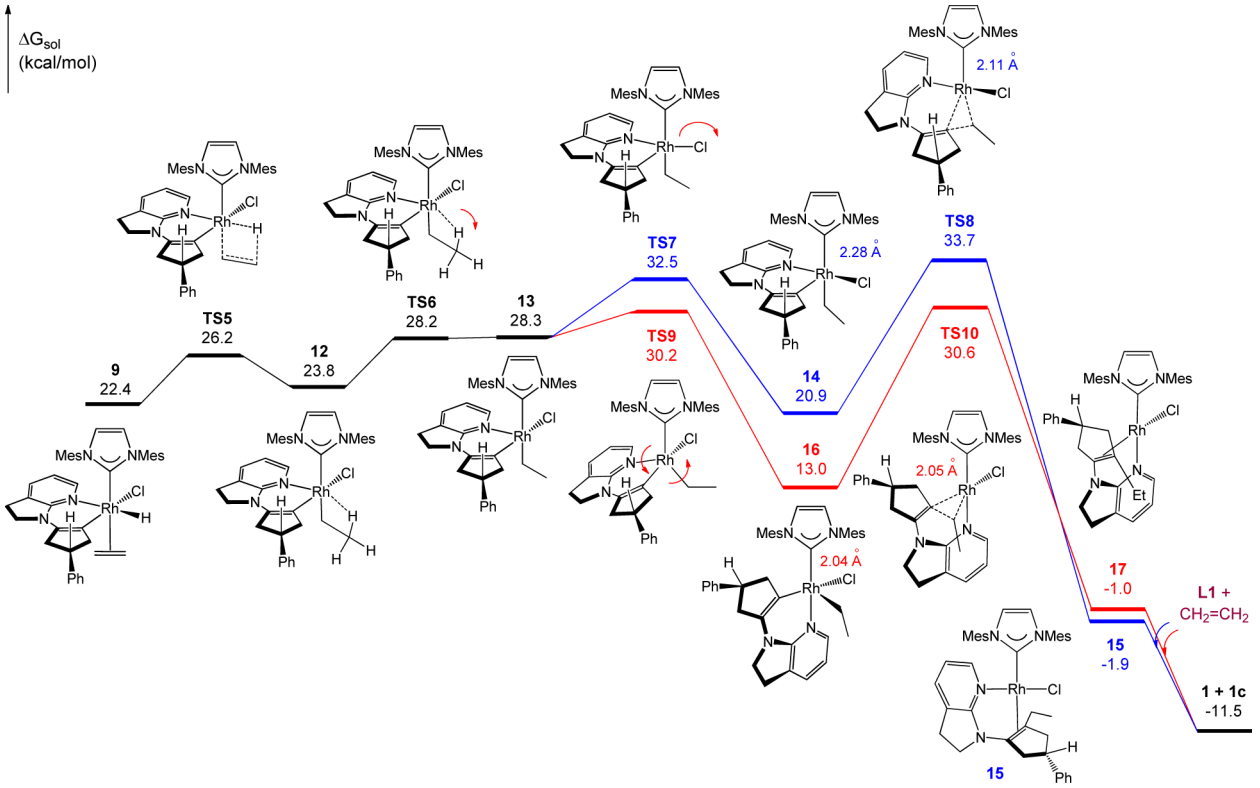

Figure 2. Free energy profiles for the enamine **1b** alkylation with ethylene mediated by **3cat**. Energies are relative to **1** + **1b** (see Figure 1) and are mass balanced.

another parallel pathway in which the Ph group points to IMes. Expectedly, due to larger steric congestion, the alternative is less favorable (*vide infra*) and we below use the favorable one to discuss the mechanism.

Starting from **3cat**, the substitution of coe (cyclooctene) ligand for the ethylene substrate, giving a Rh(I) complex **1**, is exergonic by 4.2 kcal/mol. We thus use the more stable **1**, together with **1b**, as energy reference to construct energy profiles and exclude the possibilities of forming other Rh(I) species which are more stable than **1** in Figure S3. The involvement of **1** in the present catalysis is supported by the crystallizations of its analogues.[21d,e] Then enamine **1b** coordinates to the Rh(I) center for sp^2 C−H bond activation by replacing 7-azaindoline (**L1**) and ethylene ligands, leading **1** to the less stable (13.0 and 10.6 kcal/mol, respectively) 16*e* Rh(I) complexes **2** or **3**, depending on the orientation of **1b**. Both **2** and **3** have a planar square structure, a coordination motif generally preferred by tetracoordinate Rh(I) complexes. Moreover, the coordination of **1b** to Rh(I) center is analogous to that in a X-ray characterized Rh(I) complex (complex **4** in ref 13). The bidentate coordination of **1b** in **2** and **3** showcases the two advantages of the condensation converting ketone **1a** to enamine **1b**; the coordination benefits the directionality in cleaving the targeted C^5−H bond for α-alkylation, and the conversion of the sp^3 C^α−H bond in **1a** to a sp^2 C^5−H bond in **1b** facilitates the activation of the C^5−H bond. We took both **2** and **3** into account in probing the possible catalytic pathways. In the following, we first discuss the favored one (path A1 in red) starting from **2** and then rule out the disfavored one (path A2 in blue) stemming from **3**.

By disrupting the π coordination, **2** isomerizes to an agostic complex **4** after crossing **TS1**. Although the disruption further raises the system in energy by 5.9 kcal/mol, the targeted sp^2 C^5−H bond is activated significantly, due to the donation of the C−H σ-bonding electron to the Rh(I) center, as shown by the stretched C−H bond from 1.09 Å in **2** to 1.10 Å in **TS1** to 1.20 Å in **4**. Indeed, the ensuing sp^2 C^5−H bond oxidative addition is very facile, only crossing a barrier of 2.6 kcal/mol (**TS2** relative to **4**). Subsequent to the C−H bond addition giving a Rh(III) hydride **5**, ethylene insertion into Rh(III)−H bond of **5** is about to proceed. **5** has a square pyramidal structure with a vacant coordination site opposite to the hydride. We first consider the direct coordination of ethylene to the empty site of **5**, which may result in ethylene insertion into the Rh(III)−C^5 bond, however, the insertion has a forbidden high barrier (**TS1-s**, $\Delta G^{\ddagger}$ = 59.3 kcal/mol; see Figure S4). The alternative ethylene coordinations result in high-energy structures (**6** and **7**, see Figure 1), ruling out the possibilities of inserting ethylene into Rh(III)−H bond by passing through the two complexes. Interestingly, the ethylene insertion prefers a tortuous pathway rather than a shortcut mentioned above. First, the **1b**-based ligand in **5** rotates around the Rh−C^5 bond by crossing a low barrier of 4.3 kcal/mol (**TS3** relative to **5**), placing the ligand in the equatorial plane and shifting the vacant site *trans* to IMes (see **8** in Figure 1). Then ethylene occupies the empty site, forming an 18*e* Rh(III) octahedral complex **9** that is significantly lower than **6** and **7**. Supportively, **9** features a coordination motif akin to that in a X-ray characterized Rh(III) hydride (see **RhH-exp** in Figure 1) produced from a stoichiometric reaction.[13] The organic cocatalyst **L1** can compete with ethylene to coordinate to **8**, forming **10**. Although **10** is lower than **9**, it is infertile in leading thermodynamically more favorable product. In other words, **10** is kinetically accessible but is not thermodynamically stable.

Referring to Figure 1, **3** is 2.4 kcal/mol more stable than **2**, but it cannot initiate a pathway more favorable than path A1

DOI: 10.1021/jacs.5b01502
J. Am. Chem. Soc. 2015, 137, 6279−6291

Scheme 4. Possible Pathways for Alkylations of enamine 1b and 1b′ with Ethylene[b]

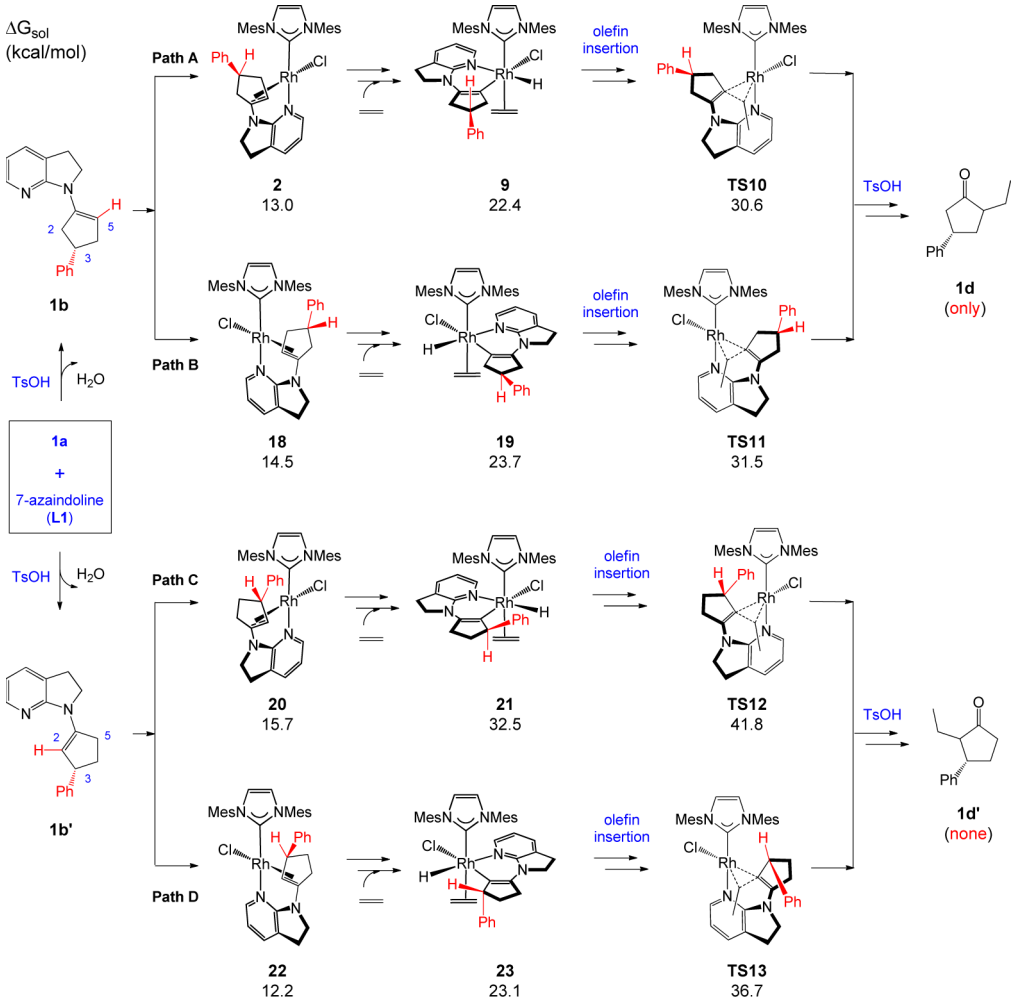

[b]The Ph-substituted carbon atoms in these structures all have the (S)-chirality.

discussed above. The barrier (**TS4**) for the intramolecular addition of the sp^2 C^5–H bond (path A2) is substantially higher than all stationary points along the favored path A1, as well as those in Figure 2 (vide infra). The higher **TS4** than **TS2** is due to the destabilization from the strong *trans*-effect between hydride and IMes ligand in **TS2**, as indicated by the longer Rh–C(IMes) bond (2.22 Å) in **TS4** than that (2.03 Å) in **TS2**. Unlike the C–H oxidative addition along path A1, no agostic interaction complex (similar to **4**) prior to **TS4** could be located probably owing to the strong *trans*-effect of IMes ligand, emphasizing the importance of preactivation via agostic coordination in this sp^2 C–H activation along path A1; **TS4** is 10.4 kcal/mol higher than **TS2**.

As shown in Figure 2, after coordinating to **8** to form the 18*e* Rh(III) π-complex **9**, ethylene inserts into the Rh(III)–H bond by spanning a low barrier of 3.8 kcal/mol (**TS5**), leading to **12** featuring a C^{β}–H bond agostic coordination to the Rh(III) center with a elongated C^{β}–H bond length (1.20 Å). An alternative ethylene insertion into the Rh(III)–C^5 bond in **9** was confirmed noncompetitive with a barrier of 45.7 kcal/mol (**TS2-s**, Figure S4). Subsequently, **12** prepares for reductive elimination to form C–C bond, converting to **13** by disabling the agostic coordination through **TS6**. Structurally, **13** could undergo reductive elimination on the site either trans or cis to IMes. Along the straightforward pathway in blue, the Cl^- ligand first steps to the site trans to pyridine ring via **TS7**, leading to more stable **14** due to the elimination of the *trans*-effect between Cl^- and C^5. Then, the reductive elimination proceeds via **TS8**, forming **15**. Along the red pathway, by crossing **TS9**, the equatorial **1b**-based ligand in **13** first rotates around Rh(III)–C^5 bond to the axial plane and the ethyl group concomitantly shifts to the equatorial plane, leading to **16** with a vacant site cis to IMes. Subsequently, reductive elimination converts Rh(III) **16** to Rh(I) **17** via **TS10**. Comparing the two pathways, the red one with reductive elimination occurring on the site cis to IMes is more favorable than the blue one with reductive elimination on the site trans to IMes. Again, the higher **14** and **TS8** than **16** and **TS10**, respectively, can be attributed to the strong *trans*-effect between IMes and ethyl group in **14** and **TS8**. Consistently, the Rh(III)–C(IMes) distances (2.28 Å/2.11 Å in **14**/**TS8**) are longer than those (2.04 Å/2.05 Å in **16**/**TS10**). It is of interest to mention that the C–H oxidative addition and the reductive elimination prefer taking place on the site cis to IMes, whereas the ethylene migratory insertion prefers the site trans to IMes. Taking the full process of the enamine **1b** alkylation into consideration, the rate-determining step of the transformation is the reductive elimination step forming C–C bond with an energy barrier of 30.6 kcal/mol (**TS10**) measured from **1** + **1b**. The relative high

DOI: 10.1021/jacs.5b01502
J. Am. Chem. Soc. 2015, 137, 6279–6291

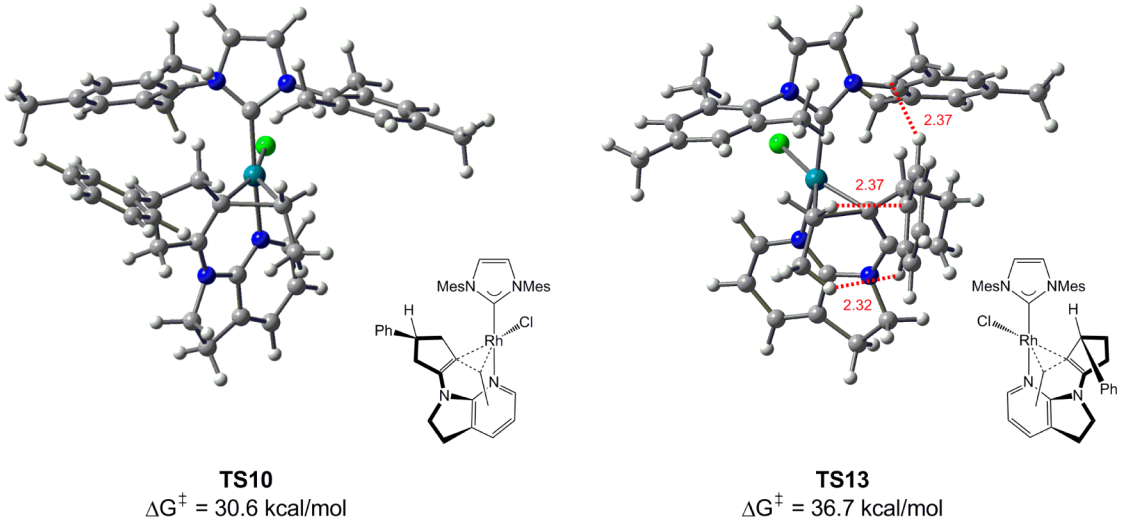

Figure 3. Optimized geometries and energy barriers for the key reductive elimination TSs **TS10** (leading to **1d**) and **TS13** (leading to **1d′**), with selected bond distances given in Å.

barrier explains the high experimental temperature (130 °C) applied for effective transformation.

Replacing the noncovalent binding **1c** ligand in **17** with **L1** and ethylene liberates **1c** and regenerates the active Rh(I) catalyst **1**. The process from **1b** to **1c** is exergonic by 11.5 kcal/mol. Under the catalysis of TsOH, enamine **1c** can be hydrated to the final α-alkylation product **1d**, which simultaneously regenerates the organic cocatalyst 7-azaindoline (**L1**). The hydrolysis process is kinetically favorable and exergonic by 9.3 kcal/mol (see Figure S2 for details). Taking the endogonicity (7.3 kcal/mol) of condensation into account, the overall catalytic α-alkylation from **1a** to **1d** is exergonic by 13.5 kcal/mol. Essentially, the α-alkylation converts π bond to σ-bond, which is the origin for the favorable thermodynamics of the alkylation.

Origins for Regioselectivity. Referring to Scheme 3, the α-alkylation of **1a** can principally take place at either the 5- or 2-site, leading to **1d** and **1d′**, respectively. On the other hand, the slightly more stable **1b′** than **1b** also implies that the transformation tends to produce **1d′**; however, only 5-site α-alkylation product **1d** was obtained.[13] To understand the regioselectivity of the reaction, we computed the pathways for the alkylation of **1b′** to **1d′** and give the complete results in Figures S6 and S7. The results affirm that the mechanism described by the red pathways in Figures 1 and 2 are also preferred for the alkylation of **1b′**. Scheme 4 compares the major results for the alkylations of **1b** and **1b′**. Note that, because of the chirality of **1b** and **1b′**, there are two pathways for each of the enantiomers (see Figures 1, 2, S5, S6, and S7 for details), depending on the orientation of Ph group, pointing toward or away from IMes. Expectedly, the alkylation of **1b** favors path A and that of **1b′** prefers path D, owing to the less steric hindrance between IMes and the Ph group in path A and path D. The rate-determining **TS10** in path A is 6.1 kcal/mol lower than its counterpart **TS13** in path D, well accounting for the experimental regioselectivity of **1d** over its regioisomer **1d′** (Figure 3). Note that the condensation giving **1b′** is only 0.4 kcal/mol thermodynamically more favorable than that giving **1b** (see above). The higher **TS13** than **TS10** can be understood by comparing their structures. In **TS10**, the Ph group points away from both IMes ligand and the coupling ethyl group, thus the steric repulsions are small if any. In contrast, the Ph group in **TS13** is toward to the ethyl group, resulting in steric hindrance between the two groups, as manifested by the significant shorter C(phenyl)···H(ethyl) distance (2.37 Å) than the sum of the van der Waals radii of C(1.70 Å) and H (1.20 Å). The H···H repulsions marked at 2.32 and 2.37 Å further destabilize **TS13**. In short, the steric hindrances between substrate−substrate and between substrate−ligand cocontribute to the observed regioselectivity of **1d**, which results in the α-alkylation occurring in the site remote to the substituted group (eq 2).[13]

Origins for Avoiding Overalkylation. It is possible that the α-alkylation product **1d** undergoes further α-alkylation to afford **1g** via the route described by eq 3; however, no overalkylation

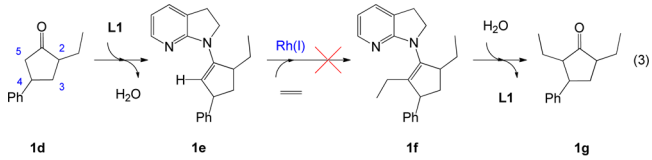

product was observed.[13] Because **1d** has already ethyl group at 2-site, the **1d** alkylation can only occur at 5-site (eq 3), which is actually similar to the 2-site α-alkylation of **1a** (Scheme 3). On the basis of the energetics for **1b′** alkylation (Scheme 4), it is not difficult to reason that the TS for further **1d** alkylation at 5-site should be higher than **TS13**, because the newly added ethyl group at 2-site of **1d** would result in additional steric hindrance, compared to **TS13** for the alkylation of **1b′**. Indeed, the reductive elimination barrier for **1d** to undergo alkylation at 5-site reaches 40.2 kcal/mol (see Figure S8 for more details), prohibiting overalkylation.

Summarizing our mechanistic discussions above, Scheme 5 outlines the mechanism for the ketone α-alkylation. The catalytic transformation proceeds via sequential seven steps, including (i) ketone **1a** condensation with the cocatalyst **L1** under the catalysis of TsOH, resulting in enamine **1b**, (ii) **1b** coordination to the Rh(I) center of active catalyst via ligand exchange, generating a Rh(I)−enamine(**1b**) intermediate **2**, (iii) intramolecular sp^2 C−H oxidative addition, leading to a Rh(III) hydride **5**, (iv) olefin coordination followed by migratory insertion, giving a Rh(III)−ethyl species **16**, (v) reductive elimination, forming C−C bond to give a Rh(I)−

DOI: 10.1021/jacs.5b01502
J. Am. Chem. Soc. 2015, 137, 6279−6291

Scheme 5. Catalytic Cycle for the Metal−Organic Cooperative Catalysis Transformation

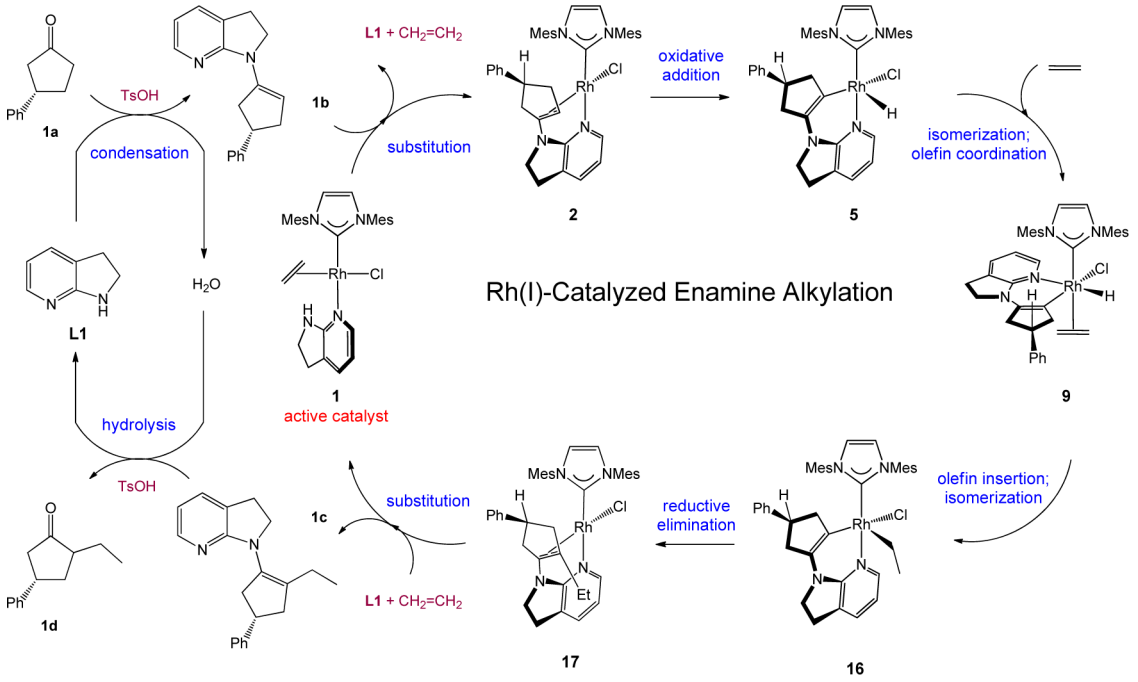

enamine (**1c**, alkylated **1b**) complex **17**, (vi) decoordination of **1c** via ligand exchange, releasing enamine **1c** (i.e., the product of **1b** alkylation) and regenerating the active catalyst **1**, and (vii) hydrolysis of **1c**, affording the final ketone α-alkylation product **1d** and regenerating the cocatalyst **L1**. Building on the mechanism and other relevant experimental evidence, we question other aspects to enrich MOCC chemistry computationally.

3.2. Why Is 7-Azaindoline (L1) So Crucial for the MOCC Transformation? Using ketone **1a** α-alkylation with ethylene as a representative, Dong et al. scrutinized the performance of several other secondary amine cocatalysts (i.e., **L2**−**L5** in Scheme 6). Thought-provokingly, **L1** worked effectively with a yield of 82% when 25 mol % **L1** was used, whereas others gave no product at all under the same experimental conditions (see Table S1 in ref 13). These experimental results emphasize the crucial role of the organic cocatalyst, but the causes behind experimental observations remained elusive. In addition, the effectiveness of an organic cocatalyst 2-amino-3-picoline (**L6**) often used in MOCC was not examined experimentally. While it could be difficult to experimentally identify the root causes for the striking difference due to the complexity of the system (e.g., because the MOCC is a cooperative process involving two catalysts, it could be difficult to quantify individual contributions of the two components experimentally), the mechanistic insight we gained can overcome the difficulty to rationalize the differences clearly. According to the mechanism, the ketone condensation with amine cocatalyst is a requisite stage (see Scheme 5), thus the thermodynamics of the condensation is a determining factor for the availability of enamine intermediates. Scheme 6 compares the thermodynamics of these condensations of ketone **1a** with different organic catalysts. The ketone condensation with **L1** is thermodynamically uphill by 7.3 kcal/mol, but it is less unfavorable than the condensations of **L2**−**L5** with ketone **1a**, which are endergonic by 15.5, 8.2, 12.4, and 12.2 kcal/mol, respectively. Furthermore, **L1** has a rate-determining barrier of 30.6 kcal/mol in the Rh(I)-catalyzed enamine **1b** alkylation, lower than those of **L2**−**L5** (32.7, 34.0, 32.6, and 32.8 kcal/mol, respectively). The substantial energetic differences in both stages accounts well for the experimental outcomes. Furthermore, the results of **L6** (2-amino-3-picoline) predict that the often-used ligand should be a less effective organic cocatalyst for ketone **1a** α-alkylation, because of its larger endogonicity (ΔG° = 9.2 kcal/mol) in the condensation stage and higher rate-determining barrier (32.3 kcal/mol) in the Rh(I)-catalyzed enamine alkylation stage.

To aid finding effective organic cocatalysts for MOCC, we analyze the major factors responsible for the different thermodynamics of these condensations. Figure 4 examines the structures of the condensation products of these ligands. The dihedral angle $\angle C^6-N-C^1-C^5$ in **1b** is 170.5°, thus the large extent of the planarity of the four atoms benefits the π(Py)−p(N)−π(C═C) conjugation, which stabilizes **1b**. Compared to **1b**, enamines **2b** and **4b** suffer from severe steric repulsions, as shown by the marked atomic distances shorter than the sum of van der Waals radii of the atoms involved. As a consequence of the steric repulsions, the extent of the planarity of the four atoms ($C^6NC^1C^5$) in **2b** and **4b** decreases, as shown by the decreased $\angle C^6-N-C^1-C^5$ angles (160.5° in **2b** and 152.2° in **4b**), which weaken the conjugation stabilization effect, further contributing to disfavoring the condensation products. Thus, the condensations of **L2** and **L4** with the ketone **1a** are more endergonic (by 15.5 and 12.4 kcal/mol, respectively) than that (7.3 kcal/mol) of **L1**. The larger endergonicities of **L3** and **L6** condensations can be rationalized similarly. Compared to **1b**, enamine **5b** produced by the condensation of [6,6]-bicyclic amine cocatalyst **L5** suffers from severer steric repulsions, as indicated by the shorter H···H distance (2.27 Å) in **5b** than the 2.42 Å in **1b**. Furthermore, the extent of planarity of the four atoms in **5b** is also significantly reduced with a dihedral angle ($\angle C^6-N-C^1-C^5$) of 150.1°. Thus, the condensation of the [6,6]-bicyclic cocatalyst (**L5**) is more endergonic than that of **L1** (7.3 vs 12.2 kcal/mol).

DOI: 10.1021/jacs.5b01502
J. Am. Chem. Soc. 2015, 137, 6279−6291

Scheme 6. Comparisons of the Thermodynamics ($\Delta G°$) of the Condensation Stage and the Kinetic Barriers ($\Delta G^{‡}$) of the Rate-Determining Step by Using Various Organic Catalysts

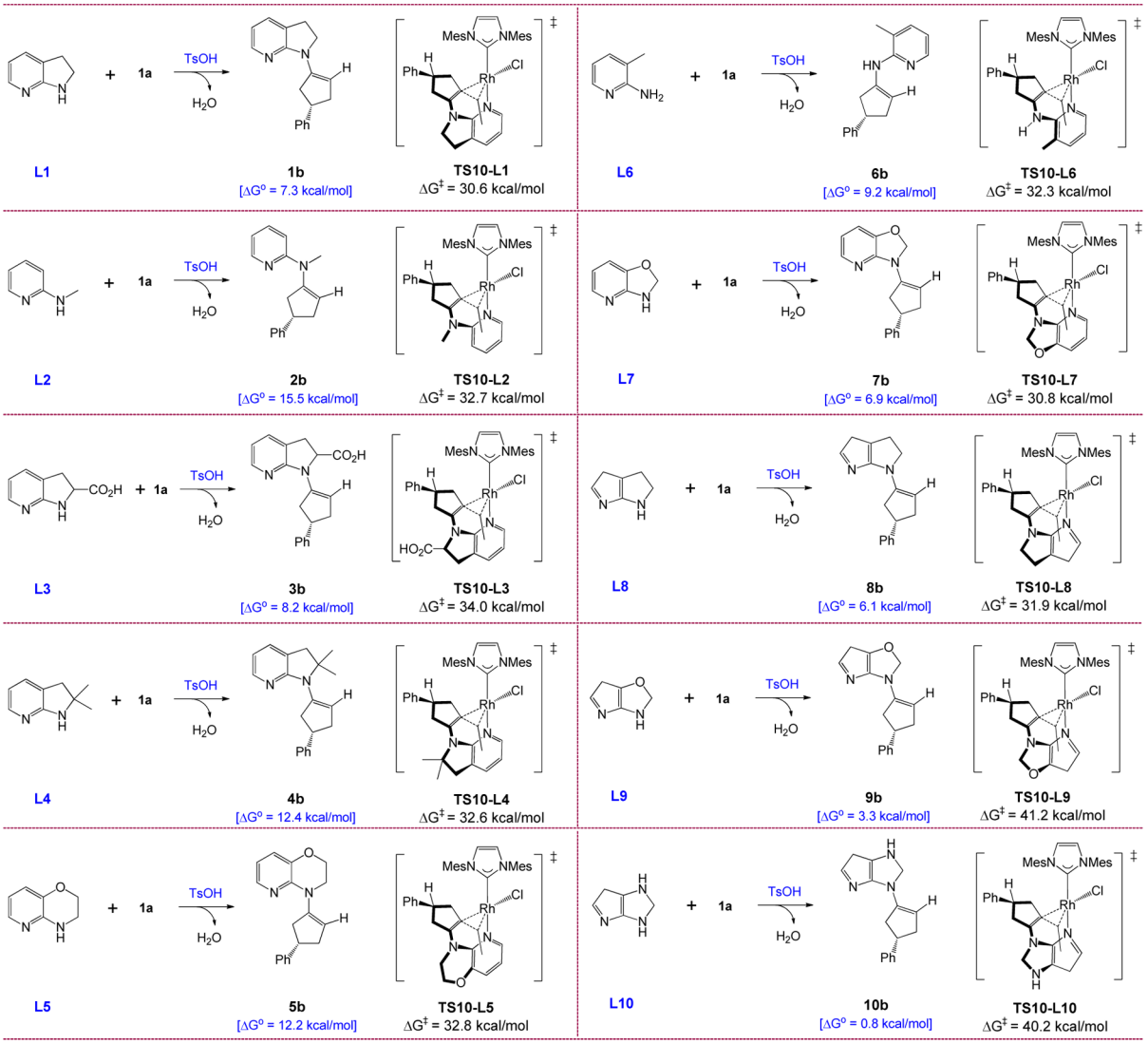

According to the analyses on **L5** ligand, we foresee that [6,6]-bicyclic secondary amines could generally not be good organic cocatlyst for such a transformation. Indeed, a serious of [6,6]-bicyclic secondary amine cocatalysts we computed all have condensation thermodynamics inferior to **L1** (see Scheme S1 for more details).

Learning from the above analyses, we envisaged that a good organic cocatalysts for the ketone alkylation should be a [6,5]- or [5,5]-bicyclic secondary amine and designed a series of such amines in attempt to improve the thermodynamics of condensation stage. Scheme 6 includes some examples (**L7**−**L10**) we computed (see Scheme S1 for more attempts). **L7** and **L8** have condensation thermodynamics slightly better than that of **L1** (6.9 and 6.1 kcal/mol versus 7.3 kcal/mol), but the resulting enamimes **7b** and **8b** are somewhat inferior (0.2 and 1.3 kcal/mol, respectively) in proceeding alkylations (see Figures S9 and S10 for complete free energy profiles). The condensations of **L9** and **L10** with **1a** are endergonic by 3.3 and 0.8 kcal/mol, respectively, thus in terms of condensation stage, **L9** and **L10** are superior to **L1**. However, the resulting condensation enamine products (**9b** and **10b**) are less kinetically favorable in proceeding alkylations, having a reductive elimination barriers (41.2 and 40.2 kcal/mol, respectively) higher than that (30.6 kcal/mol) of **L1**. The results of the two cases emphasize that, in developing an effective MOCC system, attention should be paid to both stages to reach a proper balance between the condensation and the subsequent enamine alkylation. The ligands **L7**−**L10** are designed computationally, among which **L8**−**L10** are the derivatives of iso-pyrrole. Because iso-pyrrole is less stable than pyrrole, we speculate that it could be challenging to synthesize these iso-pyrrole derivatives. Considering this, we propose that **L7** could be a good alternative for **L1** in performing ketone **1a** α-alkylation. It should be pointed out that our analyses and designs were based on ketone **1a** and a different ketone may prefer a different organic catalyst. Nevertheless, the analyses serving as examples could be borrowed to tailor an organic cocatalyst for a specific ketone α-alkylation.

3.3. Why did Wilkinson's Catalyst $RhCl(PPh_3)_3$ Exhibit Low Catalytic Activity? In the previous developments of MOCC chemistry, Wilkinson's catalyst $RhCl(PPh_3)_3$ was often employed.[7,8] Dong et al. also used the catalyst as metal component to run ketone **1a** α-alkylation. Puzzlingly, the catalyst performed poorly, with a low yield of 37% (see Table

DOI: 10.1021/jacs.5b01502
J. Am. Chem. Soc. 2015, 137, 6279−6291

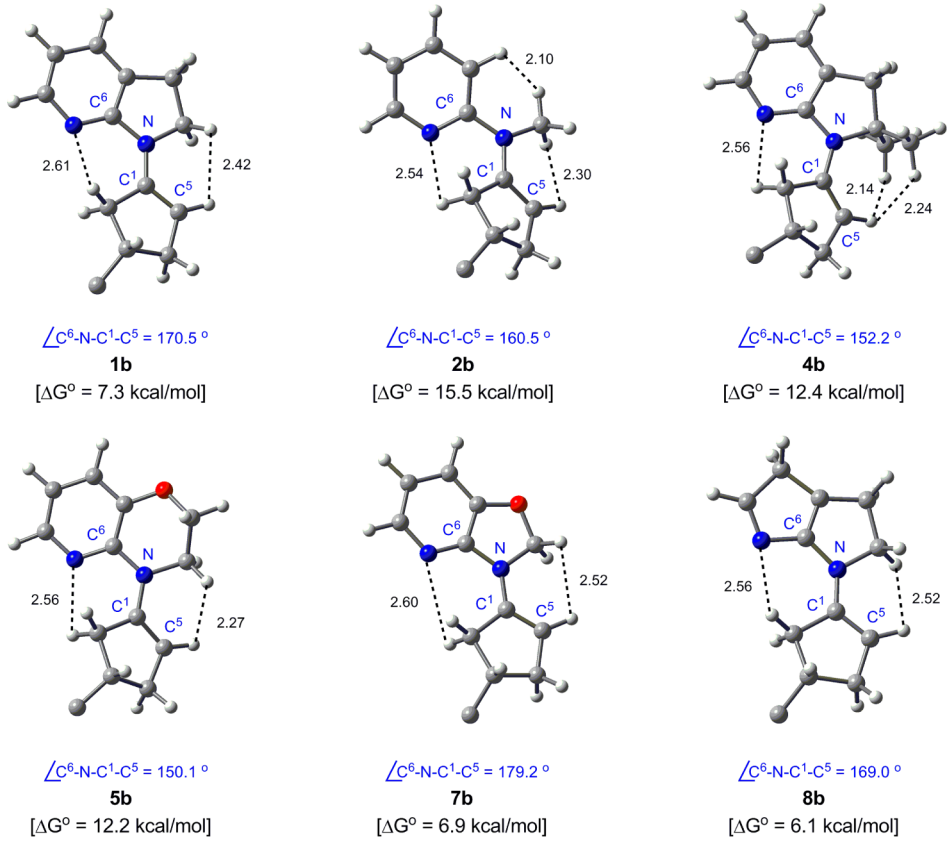

Figure 4. Optimized geometries of **1b**, **2b**, **4b**, **5b**, **7b**, and **8b**, with selected bond distances given in Å. Phenyl groups are omitted for clarity.

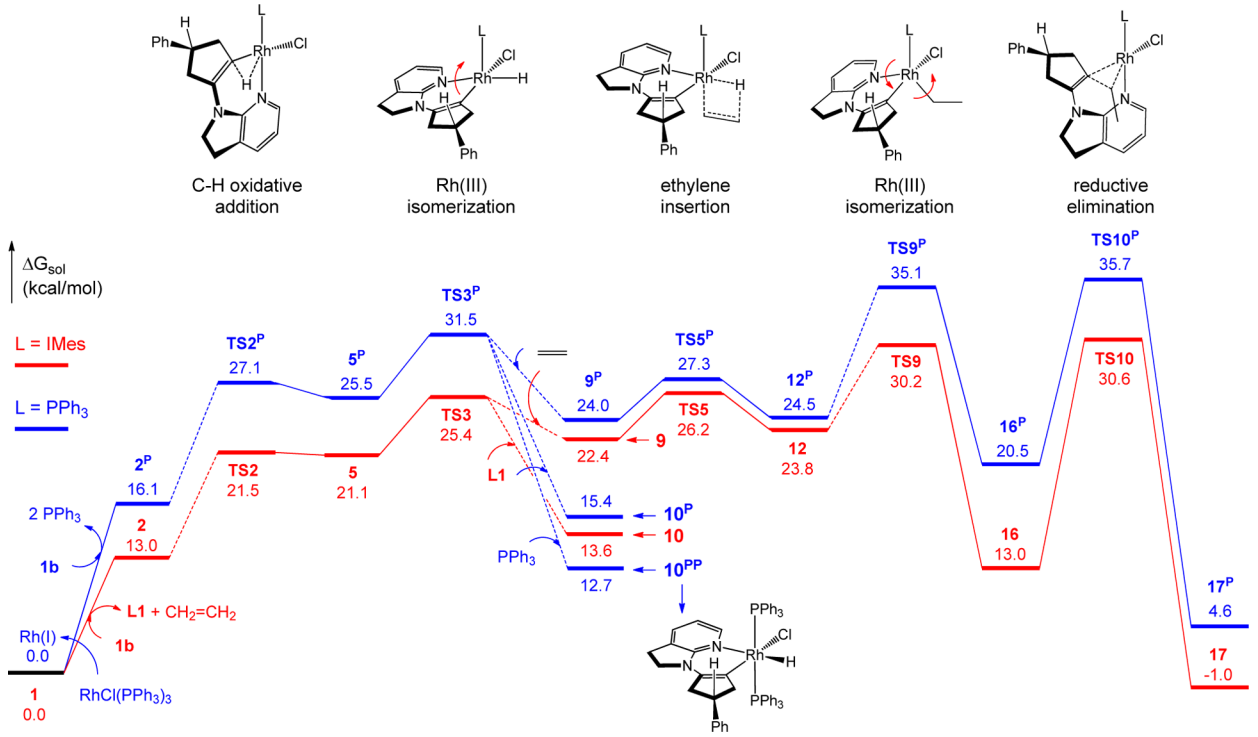

Figure 5. Free energy profiles for the enamine **1b** alkylation with ethylene catalyzed by **1** and $RhCl(PPh_3)_3$, respectively. Energies are relative to **1** + **1b** and $RhCl(PPh_3)_3$ + **1b**, respectively, and are mass balanced.

S1 in ref 13). To understand the low catalytic activity of $RhCl(PPh_3)_3$ and to further corroborate our characterized mechanism, replacing **1** with $RhCl(PPh_3)_3$, we computed the pathway for enamine **1b** alkylation. The detailed results are given in Figure S11. Figure 5 schematically compares the energetics of using **1** and $RhCl(PPh_3)_3$. The comparisons

DOI: 10.1021/jacs.5b01502
J. Am. Chem. Soc. 2015, 137, 6279−6291

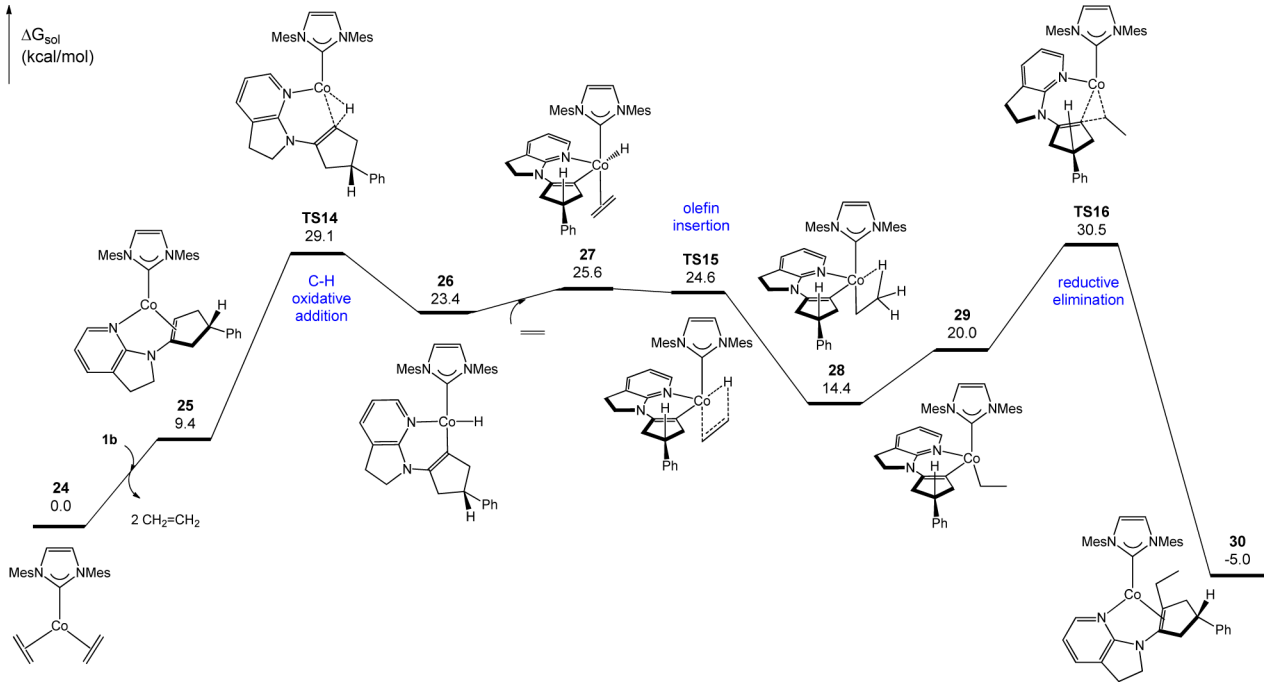

Figure 6. Free energy profile for enamine **1b** alkylation with ethylene catalyzed by IMesCo(0). Energies are relative to Co(0) complex **24** + **1b** and are mass balanced.

demonstrate that $RhCl(PPh_3)_3$ is substantially (overall by 5.1 kcal/mol) less favorable than **1** in promoting the enamine **1b** alkylation, which we attribute to the following two factors: First, $RhCl(PPh_3)_3$ is relatively more stable than **1**. As such, the enamine (**1b**) coordination to the Rh(I) center via ligand exchange giving $\mathbf{2}^{\mathbf{P}}$ is 3.1 kcal/mol (= 16.1−13.0 kcal/mol) more costly than that giving **2**. Second, PPh_3 is a weaker electron-donating ligand than IMes, which destabilizes the structures in high oxidation state (i.e., Rh(III)).

In agreement with the general notion that a weaker electron-donating ligand disfavors oxidative addition but favors reductive elimination, the net oxidative addition barrier (11.0 kcal/mol) between $\mathbf{2}^{\mathbf{P}}$ and $\mathbf{TS2}^{\mathbf{P}}$ (the blue path) is higher than the corresponding value 8.5 kcal/mol between **2** and **TS2** (the red path), while the net reductive elimination barrier (15.2 kcal/mol) between $\mathbf{16}^{\mathbf{P}}$ and $\mathbf{TS10}^{\mathbf{P}}$ is lower than the corresponding value 17.6 kcal/mol between **16** and **TS10**. Seemingly, the reduced net reductive elimination barrier from 17.6 kcal/mol (L = IMes) to 15.2 kcal/mol for L = PPh_3 contradicts to the observed lower catalytic activity of $RhCl(PPh_3)_3$ than **1**. However, the discrepancy can be reconciled by considering the fact that a weak electron-donating ligand also disfavors electron deficient structures with TM centers in the high oxidation state. Indeed, relative to IMes ligand, PPh_3 ligand destabilizes the Rh(III) complexes ($\mathbf{5}^{\mathbf{P}}$ and $\mathbf{16}^{\mathbf{P}}$) and TSs ($\mathbf{TS2}^{\mathbf{P}}$, $\mathbf{TS3}^{\mathbf{P}}$, $\mathbf{TS9}^{\mathbf{P}}$, and $\mathbf{TS10}^{\mathbf{P}}$) featuring somewhat Rh(III) characteristics; these stationary points are all higher than their counterparts (L = IMes) even though the energy difference (3.1 kcal/mol between $\mathbf{2}^{\mathbf{P}}$ and **2**) due to the different stability of the two catalysts are subtracted for considering the net electronic effects of the two ligands. Nevertheless, the energy differences between these structures ($\mathbf{9}^{\mathbf{P}}$, $\mathbf{10}^{\mathbf{P}}$, $\mathbf{TS5}^{\mathbf{P}}$, and $\mathbf{12}^{\mathbf{P}}$) and their counterparts (L = IMes) are less than 3.1 kcal/mol, indicating that PPh_3 ligand relatively stabilizes these Rh(III)-related stationary points. The seeming discrepancy can be rationalized as follow. Because these stationary points ($\mathbf{9}^{\mathbf{P}}$, $\mathbf{10}^{\mathbf{P}}$, $\mathbf{TS5}^{\mathbf{P}}$, and $\mathbf{12}^{\mathbf{P}}$) are hexacoordinate electronically saturated 18*e* Rh(III) structures, a weaker electron-donation by PPh_3 would benefit the stabilization of these electronically saturated structures. The analyses call attention to that, in choosing a proper metal ligand for a reaction with rate-determining step occurring at the reductive elimination process, a weak electron-donating ligand does decrease the net reductive elimination barrier, but does not necessarily lower the overall barrier, because a weak ligand also disfavors structures with metal center in the high oxidation state.

Because of the higher barrier, we speculate that elevated temperature may help improve the efficiency of the Wilkinson's catalyst. Furthermore, because the condensation of ketone with amine cocatalyst is endergonic, elevated temperature also benefits the stage for enamine **1b** formation.

Experimentally, Dong et al. have obtained the X-ray structure of the Rh(III)−H complex (i.e., **RhH-exp** in Figure 1) and found that the Rh(III)−H complex could not react with ethylene. The experimental facts suggest an alternative cause for the poor performance of Wilkinson's catalyst $RhCl(PPh_3)_3$. The PPh_3 ligand released in the ligand exchange could coordinate to **8**-like intermediate (referring to **8** in Figure 1) forming a stable complex ($\mathbf{10}^{\mathbf{PP}}$ in Figure 5) similar to **RhH-exp**. Because the formation of $\mathbf{10}^{\mathbf{PP}}$ is endergonic by 12.7 kcal/mol, it cannot be formed stably to affect the catalysis. In Figure S12, we rationalize why **RhH-exp** could be formed under the different experimental condition and why **RhH-exp** cannot react with ethylene.

3.4. Can Co(0)/Co(II) Redox Manifold be Used in MOCC? Surveying the reported MOCC systems including the present one, MOCC systems exclusively utilize Rh(I)/Rh(III) redox manifold. We further quest whether Co(0)/Co(II) redox manifold could be used in the MOCC-based ketone *α*-alkylation. To our knowledge, while there has been no report on Rh(0) and Ir(0) catalysis, Co(0) catalysis has been reported to perform directed C−H functionalizations.[22−24] In particular,

DOI: 10.1021/jacs.5b01502
J. Am. Chem. Soc. 2015, 137, 6279−6291

Yoshikai and co-workers reported a novel reaction of Co-catalyzed hydroarylation of 2-phenylpyridine with styrenes via chelation-assisted sp^2 C−H activation.[24e] Yoshikai et al. proposed and Fu et al. computationally showed that the hydroarylation involved IMesCo(0) as an active catalyst.[24e,25] Illuminated by these closely related precedents, we envisioned that the Co(0)/Co(II) redox manifold could be utilized to complete the catalytic cycle in a manner similar to the Rh(I) catalysis of **1**. Figure 6 shows the pathway of enamine **1b** alkylation with ethylene, catalyzed by IMesCo(0). Note that **24** is structurally different from **1** in Figure 1 and is 8.4 and 16.5 kcal/mol more stable than the complexes IMesCo(0)(**L1**)-(CH_2═CH_2) (the analogue of **1** in Figure 1) and IMesCo(0)-(**L1**)$_2$ (the analog of **4cat** in Scheme 2), respectively. We thus used **24** (doublet) and **1b** as energy reference to construct the energy profile. We have confirmed that the quartet **24** is 17.2 kcal/mol higher than the doublet **24**, indicating that the reaction would take place on the doublet energy surface (see Figure S13 for more details).[25] The pathway mainly includes three steps: sp^2 C−H oxidative addition, ethylene coordination followed by migratory insertion, and reductive elimination to form C−C bond. The C−C reductive elimination is also the rate-determining step, which is similar to the **1**-catalyzed alkylation and IMesCo(0)-mediated hydroarylation.[25] Remarkably, the rate-determining **TS16** of IMesCo(0) with $\Delta G^{\ddagger}$ = 30.5 kcal/mol is comparable with that of Rh(I) catalysis (**TS10**, $\Delta G^{\ddagger}$ = 30.6 kcal/mol), indicating that IMesCo(0) could perform the MOCC reaction. Most recently, Petit et al. reported the hydroarylation of alkynes via directed sp^2 C−H activation, using Co(0) complex (i.e., Co(PMe_3)$_4$).[24r] We also computed the pathway for enamine **1b** alkylation catalyzed by Co(PMe_3)$_4$. The results are given in Figure S14, which show that Co(PMe_3)$_4$ could behave similarly to Wilkinson's catalyst RhCl(PPh_3)$_3$. Petit et al. performed their reactions at elevated temperature (170.0 °C), thus we surmised that relatively high temperature should be applied to improve the catalytic efficiency if Co(PMe_3)$_4$ is used for MOCC reaction. Furthermore, elevated temperature also benefits the production of enamine via condensation. These computational results show the promise of using of Co(0)/Co(II) redox mainfold in developing new MOCC-based ketone α-alkylation, calling experimental realizations.

We also explored whether Co(I) and Ir(I) catalysis could be used in this MOCC system by replacing Rh in **1** with Co and Ir. The energetic results in Figure S15 indicate that the IMesCo(I)Cl and IMesIr(I)Cl complexes are unfavorable to perform the transformation.

4. CONCLUSIONS

We have performed a comprehensive DFT mechanistic study to understand the ketone α-alkylation with unactivated olefins via directed sp^3 C−H bond functionalization, catalyzed by an elaborated metal−organic cooperative catalysis (MOCC) system containing IMes-Rh(I) metal catalyst and organic cocatalyst (7-azaindoline, **L1**). The reaction proceeds via sequential seven steps, including (i) ketone **1a** condensation with the cocatalyst **L1** under the catalysis of TsOH, resulting in enamine **1b**, (ii) **1b** coordination to the Rh(I) center of active catalyst **1** via ligand exchange, generating a Rh(I)−enamine-(**1b**) intermediate **2**, (iii) intramolecular sp^2 C−H oxidative addition, leading to a Rh(III) hydride **5**, (iv) olefin coordination followed by migratory insertion, giving Rh(III)−ethyl species **16**, (v) reductive elimination, forming C−C bond to give Rh(I)−enamine (**1c**, alkylated **1b**) complex **17**, (vi) decoordination of **1c** via ligand exchange, releasing **1c** (i.e., the product of enamine **1b** alkylation) and regenerating the active catalyst **1**, and (vii) hydrolysis of **1c**, affording the final ketone α-alkylation product **1d** and regenerating the cocatalyst **L1**. The reductive elimination to form C−C bond is the rate-determining step in the whole catalytic cycle. The C−H bond preactivation through agositc interaction greatly facilitates the bond activation. Despite structurally existing a shortcut, the C−H oxidative addition and the reductive elimination prefer taking place on the site cis to IMes, whereas the ethylene migratory insertion prefers the site trans to IMes.

The established mechanism allowed us to identify the root causes behind intriguing experimental findings. The low catalytic activity of Wilkinson's catalyst RhCl(PPh_3)$_3$ is attributed to (i) the relatively great stability of the complex, which disfavors the enamine (e.g., **1b**) coordination to the Rh(I) center via ligand exchange, and (ii) the weak electron-donating PPh_3 ligand, which destabilizes some Rh(III)-related TSs and intermediates, in particular, the reductive elimination TS (**TS10**$^{\mathbf{P}}$, see Figure 5). The only success of organic cocatalyst (**L1**) and the failures of others (**L2**−**L5**) are due to that the condensation of **L1** with ketone is least endergonic and the Rh-catalyzed enamine **1b** alkylation has lowest rate-determining reductive elimination barriers (see Scheme 6).

We extended the mechanistic computations to probe new possibilities. By analyzing the root causes for the success of **L1** and the failures of **L2**−**L5**, we exemplified how to develop new organic catalysts and proposed **L7** to be a good alternative for **L1**. The pathway computations on enamine **1b** alkylations catalyzed by Co(0) complexes (e.g., IMesCo(0) and Co-(PMe_3)$_4$) demonstrate the great potential of using Co(0)/Co(II) redox manifold in developing new MOCC systems. We expect that these computational predictions can be stimulus/base to promote new experimental developments.

■ ASSOCIATED CONTENT

Supporting Information

Additional computational results, energies, and Cartesian coordinates of the optimized structures. The Supporting Information is available free of charge on the ACS Publications website at DOI: 10.1021/jacs.5b01502.

■ AUTHOR INFORMATION

Corresponding Author

*zxwang@ucas.ac.cn

Notes

The authors declare no competing financial interest.

■ ACKNOWLEDGMENTS

ZXW dedicates the paper in memory of Professor Paul von Ragué Schleyer and his contributions in popularizing the applications of computational chemistry. We acknowledge the support for this work by the National Science Foundation of China (Grant Nos. 21173263 and 21373216) and the National Basic Research Program of China (973 Program, 2015CB856500). We greatly appreciate the insightful suggestions of the anonymous reviewers which helped us to improve the study.

DOI: 10.1021/jacs.5b01502
J. Am. Chem. Soc. 2015, 137, 6279−6291

REFERENCES

(1) Selected reviews on transition-metal-catalyzed C−H functionalization: (a) Dyker, G. *Angew. Chem., Int. Ed.* **1999**, *38*, 1698. (b) Kakiuchi, F.; Murai, S. *Top. Organomet. Chem.* **1999**, *3*, 47. (c) Ritleng, V.; Sirlin, C.; Pfeffer, M. *Chem. Rev.* **2002**, *102*, 1731. (d) Labinger, J. A.; Bercaw, J. E. *Nature* **2002**, *417*, 507. (e) Kakiuchi, F.; Murai, S. *Acc. Chem. Res.* **2002**, *35*, 826. (f) Miura, M.; Nomura, M. *Top. Curr. Chem.* **2002**, *219*, 212. (g) Kakiuchi, F.; Chatani, N. *Adv. Synth. Catal.* **2003**, *345*, 1077. (h) Godula, K.; Sames, D. *Science* **2006**, *312*, 67. (i) Kakiuchi, F. *Top. Organomet. Chem.* **2007**, *24*, 1. (j) Seregin, I. V.; Gevorgyan, V. *Chem. Soc. Rev.* **2007**, *36*, 1173. (k) Alberico, D.; Scott, M. E.; Lautens, M. *Chem. Rev.* **2007**, *107*, 174. (l) Lewis, J. C.; Bergman, R. G.; Ellman, J. A. *Acc. Chem. Res.* **2008**, *41*, 1013. (m) Davies, H. M. L.; Manning, J. R. *Nature* **2008**, *451*, 417. (n) Chen, X.; Engle, K. M.; Wang, D. H.; Yu, J. Q. *Angew. Chem., Int. Ed.* **2009**, *48*, 5094. (o) Daugulis, O.; Do, H.-Q.; Shabashov, D. *Acc. Chem. Res.* **2009**, *42*, 1074. (p) Ackermann, L.; Vicente, R.; Kapdi, A. R. *Angew. Chem., Int. Ed.* **2009**, *48*, 9792. (q) Colby, D. A.; Bergman, R. G.; Ellman, J. A. *Chem. Rev.* **2010**, *110*, 624. (r) Lyons, T. W.; Sanford, M. S. *Chem. Rev.* **2010**, *110*, 1147. (s) Yeung, C. S.; Dong, V. M. *Chem. Rev.* **2011**, *111*, 1215. (t) Engle, K. M.; Mei, T.-S.; Wasa, M.; Yu, J.-Q. *Acc. Chem. Res.* **2012**, *45*, 788. (u) Yamaguchi, J.; Yamaguchi, A. D.; Itami, K. *Angew. Chem., Int. Ed.* **2012**, *51*, 8960. (v) Neufeldt, S. R.; Sanford, M. S. *Acc. Chem. Res.* **2012**, *45*, 936. (w) Rouquet, G.; Chatani, N. *Angew. Chem., Int. Ed.* **2013**, *52*, 11726. (x) Ackermann, L. *Acc. Chem. Res.* **2014**, *47*, 281. (y) Gao, K.; Yoshikai, N. *Acc. Chem. Res.* **2014**, *47*, 1208. (z) Mo, F.; Tabor, J.; Dong, G. *Chem. Lett.* **2014**, *43*, 264.

(2) (a) Mkhalid, I. A. I.; Barnard, J. H.; Marder, T. B.; Murphy, J. M.; Hartwig, J. F. *Chem. Rev.* **2010**, *110*, 890. (b) Ackermann, L. *Chem. Rev.* **2011**, *111*, 1315. (c) Cho, S. H.; Kim, J. Y.; Kwak, J.; Chang, S. *Chem. Soc. Rev.* **2011**, *40*, 5068. (d) Arockiam, P. B.; Bruneau, C.; Dixneuf, P. H. *Chem. Rev.* **2012**, *112*, 5879. (e) Colby, D. A.; Tsai, A. S.; Bergman, R. G.; Ellman, J. A. *Acc. Chem. Res.* **2012**, *45*, 814. (f) Wencel-Delord, J.; Glorius, F. *Nat. Chem.* **2013**, *5*, 369. (g) Li, B.; Dixneuf, P. H. *Chem. Soc. Rev.* **2013**, *42*, 5744. (h) Musaev, D. G.; Figg, T. M.; Kaledin, A. L. *Chem. Soc. Rev.* **2014**, *43*, 5009. (i) Cheng, G.-J.; Zhang, X.; Chung, L. W.; Xu, L.; Wu, Y.-D. *J. Am. Chem. Soc.* **2015**, *137*, 1706.

(3) (a) *C−H Activation*; Yu, J.-Q., Shi, Z.-J., Eds.; Topics in Current Chemistry, Vol. *292*; Springer: Berlin, 2010. (b) Wang, D.-H.; Engle, K. M.; Shi, B.-F.; Yu, J.-Q. *Science* **2010**, *327*, 315. (c) Leow, D.; Li, G.; Mei, T.-S.; Yu, J.-Q. *Nature* **2012**, *486*, 518. (d) Tang, R.; Li, G.; Yu, J.-Q. *Nature* **2014**, *507*, 215. (e) He, J.; Li, S.; Deng, Y.; Fu, H.; Laforteza, B. N.; Spangler, J. E.; Homs, A.; Yu, J.-Q. *Science* **2014**, *343*, 1216. (f) Liu, Y.-J.; Xu, H.; Kong, W.-J.; Shang, M.; Dai, H.-X.; Yu, J.-Q. *Nature* **2014**, *515*, 389.

(4) (a) Murai, S.; Kakiuchi, F.; Sekine, S.; Tanaka, Y.; Kamatani, A.; Sonoda, M.; Chatani, N. *Nature* **1993**, *366*, 529. (b) Kakiuchi, F.; Tanaka, Y.; Sato, T.; Chatani, N.; Murai, S. *Chem. Lett.* **1995**, 679.

(5) Colquhoun, H. M.; Thomson, D. J.; Twigg, M. V. *Carbonylation: Direct Synthesis of Carbonyl Compounds*; Plenum: New York, 1991; pp 205−225.

(6) (a) Jun, C.-H.; Lee, H.; Hong, J.-B. *J. Org. Chem.* **1997**, *62*, 1200. (b) Jun, C.-H.; Lee, D.-Y.; Hong, J.-B. *Tetrahedron Lett.* **1997**, *38*, 6673. (c) Jun, C.-H.; Lee, D.-Y.; Lee, H.; Hong, J.-B. *Angew. Chem., Int. Ed.* **2000**, *39*, 3070. (d) Jun, C.-H.; Lee, H.; Lim, S.-G. *J. Am. Chem. Soc.* **2001**, *123*, 751. (e) Jun, C.-H.; Lee, H.; Moon, C. W.; Hong, H.-S. *J. Am. Chem. Soc.* **2001**, *123*, 8600. (f) Chang, D.-H.; Lee, D.-Y.; Hong, B.-S.; Choi, J.-H.; Jun, C.-H. *J. Am. Chem. Soc.* **2004**, *126*, 424. (g) Yoo, K.; Jun, C.-H.; Hcoi, C. H.; Sim, E. *Bull. Korean Chem. Soc.* **2008**, *29*, 1920.

(7) (a) Jun, C.-H.; Moon, C. W.; Lee, D.-Y. *Chem.—Eur. J.* **2002**, *8*, 2422. (b) Jun, C.-H. *Chem. Soc. Rev.* **2004**, *33*, 610. (c) Park, Y. J.; Jun, C.-H. *Bull. Korean Chem. Soc.* **2005**, *26*, 871. (d) Jun, C.-H.; Lee, J. H. *Pure Appl. Chem.* **2004**, *76*, 577. (e) Jun, C.-H.; Jo, E.-A.; Park, J.-W. *Eur. J. Org. Chem.* **2007**, 1869.

(8) Park, Y. J.; Park, J.-W.; Jun, C.-H. *Acc. Chem. Res.* **2008**, *41*, 222.

(9) Willis, W. C. *Chem. Rev.* **2010**, *110*, 725.

(10) Ko, H. M.; Dong, G. *Nat. Chem.* **2014**, *6*, 739.

(11) (a) Iwahama, T.; Sakaguchi, S.; Ishii, Y. *Chem. Commun.* **2000**, 2317. (b) Rodriguez, A. L.; Bunlaksananusorn, T.; Knochel, P. *Org. Lett.* **2000**, *2*, 3285. (c) Pei, T.; Widenhoefer, R. A. *J. Am. Chem. Soc.* **2001**, *123*, 11290. (d) Kennedy-Smith, J. J.; Staben, S. T.; Toste, F. D. *J. Am. Chem. Soc.* **2004**, *126*, 4526. (e) Yao, X.; Li, C.-J. *J. Am. Chem. Soc.* **2004**, *126*, 6884. (f) Nakamura, M.; Hatakeyama, T.; Nakamura, E. *J. Am. Chem. Soc.* **2004**, *126*, 11820. (g) Dénès, F.; Pérez-Luna, A.; Chemla, F. *Chem. Rev.* **2010**, *110*, 2366.

(12) Wang, Z.; Reinus, B. J.; Dong, G. *J. Am. Chem. Soc.* **2012**, *134*, 13954.

(13) Mo, F.; Dong, G. *Science* **2014**, *345*, 68.

(14) (a) Lee, C. T.; Yang, W. T.; Parr, R. G. *Phys. Rev. B* **1988**, *37*, 785. (b) Becke, A. D. *J. Chem. Phys.* **1993**, *98*, 5648.

(15) (a) Andrae, D.; Häussermann, U.; Dolg, M.; Stoll, H.; Preuss, H. *Theor. Chim. Acta* **1990**, *77*, 123. (b) Roy, L. E.; Hay, P. J.; Martin, R. L. *J. Chem. Theory Comput.* **2008**, *4*, 1029.

(16) (a) Zhao, Y.; Truhlar, D. G. *Theor. Chem. Acc.* **2008**, *120*, 215. (b) Zhao, Y.; Truhlar, D. G. *Acc. Chem. Res.* **2008**, *41*, 157. (c) Zhao, Y.; Truhlar, D. G. *J. Chem. Theory Comput.* **2009**, *5*, 324. (d) Kulkarni, A. D.; Truhlar, D. G. *J. Chem. Theory Comput.* **2011**, *7*, 2325.

(17) Marenich, A. V.; Cramer, C. J.; Truhlar, D. G. *J. Phys. Chem. B* **2009**, *113*, 6378.

(18) (a) Liu, P.; Xu, X.; Dong, X.; Keitz, B. K.; Herbert, M. B.; Grubbs, R. H.; Houk, K. N. *J. Am. Chem. Soc.* **2012**, *134*, 1464. (b) Herbert, M. B.; Lan, Y.; Keitz, B. K.; Liu, P.; Endo, K.; Day, M. W.; Houk, K. N.; Grubbs, R. H. *J. Am. Chem. Soc.* **2012**, *134*, 7861. (c) Giri, R.; Lan, Y.; Liu, P.; Houk, K. N.; Yu, J.-Q. *J. Am. Chem. Soc.* **2012**, *134*, 14118. (d) Miyazaki, H.; Herbert, M. B.; Liu, P.; Dong, X.; Xu, X.; Keitz, B. K.; Ung, T.; Mkrtumyan, G.; Houk, K. N.; Grubbs, R. H. *J. Am. Chem. Soc.* **2013**, *135*, 5848. (e) Xu, X.; Liu, P.; Shu, X.-z.; Tang, W.; Houk, K. N. *J. Am. Chem. Soc.* **2013**, *135*, 9271. (f) Cannon, J. S.; Zou, L.; Liu, P.; Lan, Y.; O'Leary, D. J.; Houk, K. N.; Grubbs, R. H. *J. Am. Chem. Soc.* **2014**, *136*, 6733. (g) Haynes, M. T.; Liu, P.; Baxter, R. D.; Nett, A. J.; Houk, K. N.; Montgomery, J. *J. Am. Chem. Soc.* **2014**, *136*, 17495.

(19) (a) Tang, S.-Y.; Guo, Q.-X.; Fu, Y. *Chem.—Eur. J.* **2011**, *17*, 13866. (b) Gellrich, U.; Seiche, W.; Keller, M.; Breit, B. *Angew. Chem., Int. Ed.* **2012**, *51*, 11033. (c) Ariafard, A.; Asadollah, E.; Ostadebrahim, M.; Rajabi, N. A.; Yates, B. F. *J. Am. Chem. Soc.* **2012**, *134*, 16882. (d) Dang, Y.; Qu, S.; Wang, Z.-X.; Wang, X. *J. Am. Chem. Soc.* **2014**, *136*, 986. (e) Dang, Y.; Qu, S.; Nelson, J. W.; Pham, H. D.; Wang, Z.-X.; Wang, X. *J. Am. Chem. Soc.* **2015**, *137*, 2006.

(20) Frisch, M. J. et al. *Gaussian 09*, revision A.01; Gaussian, Inc.: Wallingford, CT, 2009.

(21) (a) Yu, X. Y.; Patrick, B. O.; James, B. R. *Organometallics* **2006**, *25*, 4870. (b) Zenkina, O. V.; Keske, E. C.; Wang, R.; Crudden, C. M. *Organometallics* **2011**, *30*, 6423. (c) Zenkina, O. V.; Keske, E. C.; Wang, R.; Crudden, C. M. *Angew. Chem., Int. Ed.* **2011**, *50*, 8100. (d) Di Giuseppe, A.; Castarlenas, R.; Pérez-Torrente, J. J.; Crucianelli, M.; Polo, V.; Sancho, R.; Lahoz, F. J.; Oro, L. A. *J. Am. Chem. Soc.* **2012**, *134*, 8171. (e) Azpíroz, R.; Rubio-Pérez, L.; Di Giuseppe, A.; Passarelli, V.; Lahoz, F. J.; Castarlenas, R.; Pérez-Torrente, J. J.; Oro, L. A. *ACS Catal.* **2014**, *4*, 4244.

(22) Kulkarni, A. A.; Daugulis, O. *Synthesis* **2009**, 4087.

(23) For recent reviews on Co-catalyzed C−H functionalization: (a) Gao, K.; Yoshikai, N. *Acc. Chem. Res.* **2014**, *47*, 1208. (b) Tilly, D.; Dayaker, G.; Bachu, P. *Catal. Sci. Technol.* **2014**, *4*, 2756.

(24) Selected examples on Co-catalyzed C−H functionalization: (a) Bolig, A. D.; Brookhart, M. *J. Am. Chem. Soc.* **2007**, *129*, 14544. (b) Gao, K.; Lee, P.-S.; Fujita, T.; Yoshikai, N. *J. Am. Chem. Soc.* **2010**, *132*, 12249. (c) Li, B.; Wu, Z.-H.; Gu, Y.- F.; Sun, C.-L.; Wang, B.-Q.; Shi, Z.-J. *Angew. Chem., Int. Ed.* **2011**, *50*, 1109. (d) Gao, K.; Yoshikai, N. *Angew. Chem., Int. Ed.* **2011**, *50*, 6888. (e) Gao, K.; Yoshikai, N. *J. Am. Chem. Soc.* **2011**, *133*, 400. (f) Chen, Q.; Ilies, L.; Nakamura, E. *J. Am. Chem. Soc.* **2011**, *133*, 428. (g) Ilies, L.; Chen, Q.; Zeng, X.; Nakamura, E. *J. Am. Chem. Soc.* **2011**, *133*, 5221. (h) Lee, P.-S.; Fujita, T.; Yoshikai, N. *J. Am. Chem. Soc.* **2011**, *133*, 17283. (i) Gao, K.; Yoshikai, N. *Chem. Commun.* **2012**, *48*, 4305. (j) Yao, T.; Hirano, K.;

DOI: 10.1021/jacs.5b01502
J. Am. Chem. Soc. 2015, 137, 6279−6291

Satoh, T.; Miura, M. *Angew. Chem., Int. Ed.* **2012**, *51*, 775. (k) Ding, Z.; Yoshikai, N. *Angew. Chem., Int. Ed.* **2012**, *51*, 4698. (l) Song, W.; Ackermann, L. *Angew. Chem., Int. Ed.* **2012**, *51*, 8251. (m) Andou, T.; Saga, Y.; Komai, H.; Matsunaga, S.; Kanai, M. *Angew. Chem., Int. Ed.* **2013**, *52*, 3213. (n) Punji, B.; Song, W.; Shevchenko, G. A.; Ackermann, L. *Chem.—Eur. J.* **2013**, *19*, 10605. (o) Xu, W.; Yoshikai, N. *Angew. Chem., Int. Ed.* **2014**, *53*, 14166. (p) Chen, Q.-A.; Kim, D. K.; Dong, V. Y. *J. Am. Chem. Soc.* **2014**, *136*, 3772. (q) Zhao, C.; Crimmin, M. R.; Toste, F. D.; Bergman, R. G. *Acc. Chem. Res.* **2014**, *47*, 517. (r) Fallon, B. J.; Derat, E.; Amatore, M.; Aubert, C.; Chemla, F.; Ferreira, F.; Pérez-Luna, A.; Petit, M. *J. Am. Chem. Soc.* **2015**, *137*, 2448.

(25) Yang, Z.; Yu, H.; Fu, Y. *Chem.—Eur. J.* **2013**, *19*, 12093.

DOI: 10.1021/jacs.5b01502
J. Am. Chem. Soc. 2015, 137, 6279−6291